Geophysical Journal International

Geophys. J. Int. (2020) **223,** 1644–1657
Advance Access publication 2020 August 22
GJI Seismology

doi: 10.1093/gji/ggaa398

A joint inversion of receiver function and Rayleigh wave phase velocity dispersion data to estimate crustal structure in West Antarctica

C.K. Dunham,[1] J.P. O'Donnell,[1] G.W. Stuart,[1] A.M. Brisbourne,[2] S. Rost,[1] T.A. Jordan,[2] A.A. Nyblade,[3] D.A. Wiens[4] and R.C. Aster[5]

[1]*School of Earth and Environment, The University of Leeds, Leeds LS29JT, UK. E-mail: c.k.dunham@leeds.ac.uk*
[2]*British Antarctic Survey, National Environment Research Council, Cambridge, CB30ET, UK*
[3]*Department of Geosciences, The Pennsylvania State University, University Park, PA 16802, USA*
[4]*Department of Earth and Planetary Sciences, Washington University, St. Louis, MO 63160, USA*
[5]*Department of Geosciences, Colorado State University, Fort Collins, CO 80523, USA*

Accepted 2020 August 21. Received 2020 July 21; in original form 2020 January 15

SUMMARY

We determine crustal shear wave velocity structure and crustal thickness at recently deployed seismic stations across West Antarctica, using a joint inversion of receiver functions and fundamental mode Rayleigh wave phase velocity dispersion. The stations are from both the UK Antarctic Network (UKANET) and Polar Earth Observing Network/Antarctic Network (POLENET/ANET). The former include, for the first time, four stations along the spine of the Antarctic Peninsula, three in the Ellsworth Land and five stations in the vicinity of the Pine Island Rift. Within the West Antarctic Rift System (WARS) we model a crustal thickness range of 18–28 km, and show that the thinnest crust (∼18 km) is in the vicinity of the Byrd Subglacial Basin and Bentley Subglacial Trench. In these regions we also find the highest ratio of fast (V_s = 4.0–4.3 km s^{-1}, likely mafic) lower crust to felsic/intermediate upper crust. The thickest mafic lower crust we model is in Ellsworth Land, a critical area for constraining the eastern limits of the WARS. Although we find thinner crust in this region (∼30 km) than in the neighbouring Antarctic Peninsula and Haag-Ellsworth Whitmore block (HEW), the Ellsworth Land crust has not undergone as much extension as the central WARS. This suggests that the WARS does not link with the Weddell Sea Rift System through Ellsworth Land, and instead has progressed during its formation towards the Bellingshausen and Amundsen Sea Embayments. We also find that the thin WARS crust extends towards the Pine Island Rift, suggesting that the boundary between the WARS and the Thurston Island block lies in this region, ∼200 km north of its previously accepted position. The thickest crust (38–40 km) we model in this study is in the Ellsworth Mountain section of the HEW block. We find thinner crust (30–33 km) in the Whitmore Mountains and Haag Nunatak sectors of the HEW, consistent with the composite nature of the block. In the Antarctic Peninsula we find a crustal thickness range of 30–38 km and a likely dominantly felsic/intermediate crustal composition. By forward modelling high frequency receiver functions we also assess if any thick, low velocity subglacial sediment accumulations are present, and find a 0.1–0.8-km-thick layer at 10 stations within the WARS, Thurston Island and Ellsworth Land. We suggest that these units of subglacial sediment could provide a source region for the soft basal till layers found beneath numerous outlet glaciers, and may act to accelerate ice flow.

Key words: Antarctica; Joint inversion; Crustal structure.

1 INTRODUCTION

West Antarctica has an enigmatic tectonic history, and is host to one of the largest continental rift systems on Earth—The West Antarctic Rift System (WARS, Dalziel & Elliot 1982). The size and total amount of extension encompassed by the WARS is still unclear due to the overlying West Antarctic Ice Sheet; this uncertainty has implications for accurately achieving global plate circuit closure in tectonic reconstructions. The WARS features deep bedrock elevations (Fretwell *et al.* 2013) and thin crust (Chaput *et al.* 2014), formed as a result of late Mesozoic and Cenozoic extension between East and West Antarctica (e.g. Fitzgerald 2002, and references therein). The possible eastern progression of the WARS through Ellsworth Land is seismically poorly constrained; studies suggest that it variably extends into both the Bellingshausen and Amundsen Sea embayments (e.g. Gohl *et al.* 2015; Kalberg *et al.* 2015) and as far as the George VI Sound (Eagles *et al.* 2009). It is also unclear if there is a linkage between the WARS and the neighbouring Weddell Sea Rift System, a broad extensional province spanning the boundary between East and West Antarctica (Jordan *et al.* 2017). In addition to the WARS, West Antarctica is comprised of a mosaic of antecedent crustal blocks separated by the rift system, each with a distinct tectonic history. These are the Antarctic Peninsula, Thurston Island, Haag-Ellsworth Whitmore (HEW) and Marie Byrd Land blocks (Fig. 1).

In this study, we use a joint inversion of receiver function and Rayleigh wave phase velocity dispersion data from UKANET and POLENET/ANET seismic stations across West Antarctica. The UKANET deployment includes stations in the southern Antarctic Peninsula and Ellsworth Land for the first time. These stations will provide valuable insight into the eastern termination of the WARS, and whether there is a connection between the WARS and the Weddell Sea Rift System. Additionally, we include stations from the UKANET–POLENET/ANET Mini Array traverse which straddle the Thurston Island-WARS boundary, which will allow for a better delineation of the northern edge of the WARS and its progression towards the Amundsen Sea Embayment. By recovering a shear wave velocity–depth profile at each station we aim to constrain both crustal thickness as well as the relative proportions of likely felsic/intermediate to mafic crust. We consider the crustal structure we model at each station relative to its respective crustal block, then evaluate the overall tectonic framework with regards to global analogues.

Another feature we aim to model is the presence of low seismic velocity subglacial sediment accumulations beneath the West Antarctic Ice Sheet. The basal environment of the ice sheet plays a key role in its future stability; two important controls on ice sheet models are basal heat flow and friction. Sediment accumulations can provide a source region for basal till generation, which in turn has been proposed to be necessary for the initiation of fast ice flow (Blankenship *et al.* 2001). As such, the location of thick subglacial sediment accumulation can give an indication of likely or unlikely areas of fast ice flow. Subglacial sediment has been inferred beneath sections of the West Antarctic Ice Sheet by previous receiver function studies (Winberry & Anandakrishnan 2004; Chaput *et al.* 2014), with estimates of sediment thickness up to 0.6 km in the Bentley Subglacial Trench and 0.3 km in the Byrd Subglacial Basin. With the recently collected data used in this study we aim to determine the distribution of major subglacial sediment accumulations across West Antarctica.

2 TECTONIC SETTING

Antarctica can be broadly divided into two tectonic domains divided by the Transantarctic Mountains (TAM). East Antarctica features a thick Archean-Proterozoic cratonic crust, whilst West Antarctica consists of a mosaic of crustal blocks with a varied history (e.g. Dalziel 1992). The Antarctic Peninsula, Thurston Island and Marie-Byrd Land are Palaeozoic–Mesozoic accreted terranes which formed along the palaeo-Pacific Gondwanan margin, abutting East Antarctica (Dalziel & Elliot 1982). The Jurassic breakup of Gondwana led to the development of the Weddell Sea Rift System (e.g. Jordan *et al.* 2017), and subsequent Cretaceous-to-Cenozoic extension between East Antarctica and Marie Byrd Land produced the WARS. In addition the HEW block, which is considered a composite fragment of cratonic Gondwanan crust, was translated and rotated into its current position following the break up of Gondwana.

2.1 Haag-Ellsworth Whitmore block

The HEW is a composite block consisting of the Haag-Nunataks, Ellsworth Mountains and Whitmore Mountains. The block features atypical stratigraphy and crustal structure with respect to its surroundings, and is proposed to be a remnant of Gondwanan lithosphere. The northwest–southeast structural trend within the HEW is perpendicular to the neighbouring Thiel Mountains, which are part of the TAM (Storey & Dalziel 1987), suggesting that it has undergone significant rotation (Dalziel & Elliot 1982). The HEW predominantly consists of clastic metasedimentary rock with isolated igneous intrusions. Models of how the HEW arrived at its current position are contentious. Palaeomagnetic and geological interpretations (Schopf 1969; Randall & Mac Niocaill 2004) include a 90° anticlockwise rotation and ∼1500 km of translation from a pre-rift position between South Africa and East Antarctica. A more recent geophysical study of the Weddell Sea by Jordan *et al.* (2017) proposes a 'less travelled' model, whereby the HEW was originally located in the Weddell Sea region before Jurassic extension. The model of Jordan *et al.* (2017) only accounts for a ∼30° rotation, but they suggest that deformation associated with the Permian Gondwanide Orogen may have provided the additional rotation required to reconcile with previous observations.

2.2 Antarctic Peninsula and Thurston Island

The Antarctic Peninsula and Thurston Island evolved via sustained back arc magmatism and accretion due to the subduction of the Phoenix Plate beneath the Antarctic Plate, before experiencing Cenozoic and Mesozoic uplift (Birkenmajer *et al.* 1986; Grunow *et al.* 1991; Machado *et al.* 2005). To restore the Antarctic Peninsula to its pre-Gondwanan break up position it must be rotated anticlockwise with respect to East Antarctica, eventually aligning with the southern tip of South America (Fitzgerald 2002). Modelling of radiogenic heat flux suggests that the more silicic south and east of the Antarctic Peninsula have a higher heat flux (∼81 mW m^{-2}) than the north and west (∼67 mW m^{-2}, Burton-Johnson *et al.* 2017).

2.3 West Antarctic Rift System (WARS)

The WARS is an asymmetric rift system 750–1000 km in width and 3000 km in length (Behrendt *et al.* 1991). The WARS developed as a consequence of predominately Cretaceous extension as the Antarc-

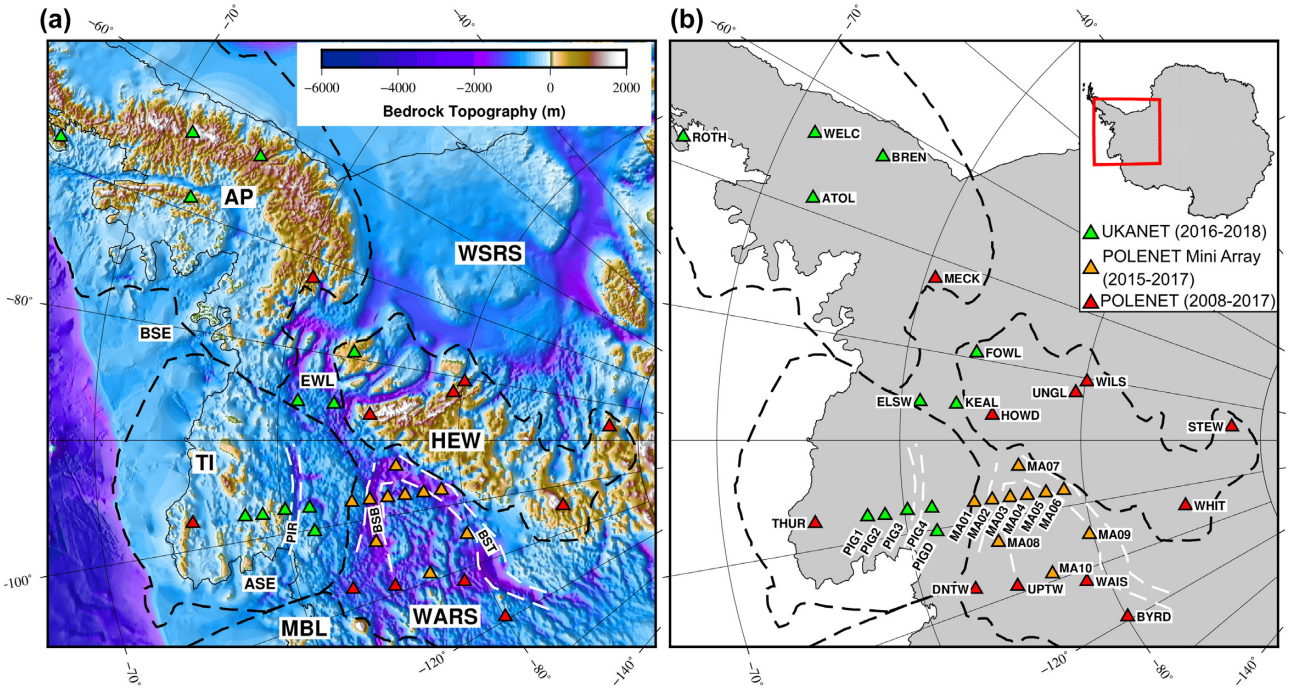

Figure 1. Maps of our study area in West Antarctica. (a) BEDMAP2 bedrock topography (Fretwell *et al.* 2013) with the crustal block boundaries of Dalziel & Elliot (1982) displayed with black dashed lines. The crustal blocks are as follows: Antarctic Peninsula (AP), Thurston Island (TI), Marie Byrd Land (MBL), Haag-Ellsworth Whitmore block (HEW). Also included are West Antarctic Rift System (WARS), Weddell Sea Rift System (WSRS), Ellsworth Land (EWL), Amundsen Sea Embayment (ASE) and Bellingshausen Sea Embayment (BSE). Major regional structures shown with white dashed lines are the Byrd Subglacial Basin (BSB), Bentley Subglacial Trench (BST) and Pine Island Rift (PIR). (b) A map highlighting the stations used in this study. The UKANET seismic network (2016–2018) is shown in green triangles, the POLENET/ANET Mini Array (2015–2017) in orange and POLENET/ANET longer term (2008–) stations in red.

tic Peninsula, Thurston Island and Marie Byrd Land moved away from East Antarctica. It has been proposed that extension occurred in two pulses; the major phase being a well documented period of broad extension across the whole WARS in the Jurassic–Cretaceous (Luyendyk 1995; Siddoway *et al.* 2004). A second pulse of extension in the Neogene has been inferred in the sedimentary basins of the Ross Sea (e.g. Behrendt 1999; Wilson & Luyendyk 2006), although to what extent the entire WARS was impacted is unclear. Although Neogene extension appears to be preferentially concentrated along the East–West Antarctic boundary (e.g. Harry *et al.* 2018), some geophysical studies have inferred concurrent extension in central and eastern portions of the WARS (e.g. Winberry & Anandakrishnan 2004; Jordan *et al.* 2010; Damiani *et al.* 2014). Lloyd *et al.* (2015) also interpreted reduced seismic wave speeds in the uppermost mantle beneath the WARS as the remnant thermal signal of localized Neogene rifting. It has been proposed that WARS extension slowed at *ca*. 17 Ma (Granot *et al.* 2013). The lack of recent significant seismicity in the region (e.g. Reading 2007) combined with the very low rates of tectonic intraplate deformation (Donnellan & Luyendyk 2004; Barletta *et al.* 2018), suggest that the WARS is currently nearly inactive.

Given the ambiguity over the timing of extension and the substantial ice cover, estimates of total extension encompassed by the WARS are poorly constrained. In the Ross Sea one-layer crustal stretching models assuming a ∼35 km initial thickness compared to the presently estimated 17–27-km-thick crust suggest ∼400 km of extension (e.g. Behrendt & Cooper 1991), whilst palaeomagnetic modelling (DiVenere *et al.* 1994) indicates a range from 440 to 1820 km. Palaeomagnetic studies in this region are hampered by uncertainties in the amount of rotation between West Antarctica's crustal blocks, and a lack of Cretaceous correlative poles. Improving estimates of crustal thickness within the WARS will allow for more accurate modelling of the total extension.

2.4 Recent geophysical investigation of crustal structure in West Antarctica

Thanks to the gradual improvement in data coverage over the past 20 yr, gravity studies have provided valuable insight into Antarctica's tectonic structure (e.g. von Frese *et al.* 1999; Llubes *et al.* 2003; Block *et al.* 2009; Jordan *et al.* 2010; O'Donnell & Nyblade 2014). By inverting GRACE satellite gravity data Block *et al.* (2009) modelled crust up to 46 km thick in East Antarctica and ∼30 km in the centre of the WARS. O'Donnell & Nyblade (2014) followed this study using an inversion of GOCO03S satellite gravity data, finding a mean crustal thickness of 40 km in East Antarctica and 24 km in West Antarctica. Aerogravity has been used in more localized studies to image shorter wavelength structure. Jordan *et al.* (2010) focused on the Pine Island Glacier region and model crust as thin as 19 km, suggesting that the region has been subject to enhanced crustal thinning.

Since the deployment of POLENET/ANET, a number of studies have used the network to investigate crustal structure across West Antarctica. Chaput *et al.* (2014) produced *P*-wave receiver functions from the POLENET/ANET deployment and inverted them for crustal structure using a Markov Chain Monte Carlo approach. They found 20–25-km-thick crust in the central WARS, surrounded by thicker adjacent crustal blocks: ∼35 km in the HEW block, ∼30 km in Marie Byrd Land, and up to 45 km in the TAM. Additionally,

Chaput *et al.* (2014) inferred a layer of low velocity subglacial sediment at many stations, with a thickness of up to ∼0.4 km within the Bentley Subglacial Trench. The presence of subglacial sediment in the region had previously been suggested by Anandakrishnan & Winberry (2004), who inferred a ∼0.6-km-thick layer in the vicinity of the Bentley Subglacial Trench.

To avoid the complex near surface reverberation present in *P*-wave receiver functions for stations on thick ice sheets, Ramirez *et al.* (2016) used *S*-to-*P* receiver functions at POLENET/ANET stations across West Antarctica. They found crustal thickness to be in general agreement with Chaput *et al.* (2014), varying from 19 to 29 km across the WARS. Ramirez *et al.* (2017) built upon this study by using a joint inversion of Rayleigh wave phase velocities and *P*-wave receiver functions to image crustal structure at bedrock stations in West Antarctica. They reported average crustal thicknesses of ∼37 km in the HEW, ∼30 km in Marie Byrd Land, 35 km at station MECK in the southern Antarctic Peninsula and 38 km at THUR on the Thurston Island block. Crustal thickness from Ramirez *et al.* (2017) generally agree with Chaput *et al.* (2014), however they estimated the crust to be ∼10 km thicker at stations MECK and THUR, which they attributed to the presence of a 10–20-km-thick mafic lower crust.

Shen *et al.* (2018) combined fundamental mode Rayleigh wave phase and group velocity dispersion and receiver functions in a Bayesian Monte Carlo algorithm to construct a 3-D shear velocity model of the crust and uppermost mantle across Antarctica. In the WARS they find crustal thickness to range from 20 to 30 km, which is consistent with aforementioned studies. Additionally, Shen *et al.* (2018) image thinner crust and upper mantle low velocity anomalies in the Amundsen Sea Embayment and Byrd Subglacial Basin, suggesting that these regions have experienced recent extension. O'Donnell *et al.* (2019a) and O'Donnell *et al.* (2019b) modelled fundamental mode Rayleigh wave phase velocities at periods 7–143 s across West Antarctica using seismic ambient noise and earthquake data recorded on the UKANET and POLENET/ANET stations. O'Donnell *et al.* (2019a) find ∼22-km-thick extended crust in the Ross and Amundsen Sea Embayments, and suggest that the Cenozoic evolution of the WARS shows along strike variability. In addition, O'Donnell *et al.* (2019a) model crust to be ∼32–35 km thick in the southern Antarctic Peninsula and ∼30–40 km thick in the HEW.

3 DATA AND METHODS

3.1 Stations

The data used in this study were recorded on 33 stations (see Table S1) distributed across the eastern WARS, Thurston Island, HEW and southern Antarctic Peninsula from the UKANET (2016–2018) and POLENET/ANET (2008–) seismic networks (Fig. 1). The stations are situated on ice as well as on bedrock, with rock sites typically on the flanks of nunataks. POLENET/ANET consists of long-term backbone stations distributed across West Antarctica, which feature a mixture of cold-rated Guralp CMG-3T 120 s and Nanometrics Trillium 240 s sensors, sampling at 1 and 40 samples per second (sps). The UKANET (2016–2018) and POLENET-ANET mini-array (2015–2017) were denser but shorter term deployments, with the former featuring Guralp CMG-3T 120 s seismometers which sampled at 1 and 100 sps, and the latter Nanometrics 120 s PH sensors.

3.2 Receiver functions

P-wave receiver function analysis is a powerful tool for estimating depths to significant seismic impedance contrasts beneath the receiver, and are produced at each station via a deconvolution of the vertical from the radial component for teleseismic earthquakes (e.g. Langston 1979). For receiver function analysis, we use teleseismic earthquakes in the epicentral distance range of 30° to 90° with magnitude $M_w \geq 5.8$ from 2008 to 2018. Prior to deconvolution we cut each seismogram from 10 s before to 120 s after the theoretical *P*-wave arrival according to the IASP91 global model (Kennett & Engdahl 1991), and then detrend, taper and high pass filter at 0.05 Hz. We rotate the east and north components of the seismogram to the great circle path to produce radial and transverse components, then compute receiver functions using the Extended Multi-Taper Receiver Function (ETMTRF) method of Helffrich (2006). ETMTRF has successfully been applied at noisy stations, such as in ocean island studies (Lodge & Helffrich 2009) where the noise conditions are similar to the Antarctic Peninsula (Anthony *et al.* 2015).

We produce receiver functions at three maximum frequencies: 0.5, 2 and 4 Hz. The 0.5 and 2 Hz maximum frequency receiver functions are used in the joint inversion, whilst the 4 Hz receiver functions are used in forward modelling for subglacial sediment. The 0.5 Hz maximum frequency receiver functions will improve our observation of deeper structure, whilst the higher frequency receiver functions offer better resolution of the near surface ice/sediment (e.g. Piana Agostinetti & Malinverno 2018). Strong multiple reverberations (Fig. 2) complicate the time series and arise when thin low velocity layers, such as ice and sediment, are present beneath the seismic station. These ice/sediment reverberations can interfere with important crustal phases from the Moho (e.g. Ps_{Moho}). Fig. 2 shows 2 Hz receiver functions generated from 2016 to 2018 at UKANET station PIG1 binned by slowness and backazimuth. The early portion of the receiver function is influenced by the *P*-wave reverberation in the ice/subglacial sediment layers, contaminating the expected arrival of crustal phases, for example Ps_{Moho}. For a 30-km-thick crust the Ps_{Moho} phase would be expected to arrive at 3–4 s, whilst the often-high amplitude reflected phases from the base of the ice sheet could arrive at roughly the same time depending on ice thickness.

3.3 Forward modelling to infer subglacial sediment

We forward model high frequency receiver functions to detect if any subglacial sediment is present at each station. Ice thickness is constrained to less than ±100 m by BEDMAP2 (Fretwell *et al.* 2013) at most stations, and is treated as a uniform layer in the forward modelling. Ice velocity is fixed at $V_p = 3.87$ km s^{-1}, $V_s = 1.9$ km s^{-1} and density at $\rho = 0.9$ g cm^{-3} based on seismic studies of polar ice (Kohnen 1974).

We use the grid search forward modelling approach of Anandakrishnan & Winberry (2004) to characterize any potential subglacial sediment (Fig. 3). We allow subglacial sediment thickness to vary from 0 to 1 km, and V_s from 0.2 to 2.0 km s^{-1}; V_p and ρ are calculated using the empirical relations defined by Brocher (2005). A synthetic receiver function is generated, having been preprocessed and deconvolved with the same parameters as the data at a maximum frequency of 4 Hz. To analyse model fit we compute the L_2 norm residual between the synthetic and observed stacked 4 Hz receiver function over the first 4 s. By analysing misfit over the first 4 s we aim to exploit the shift in the relative timing of the ice conversions

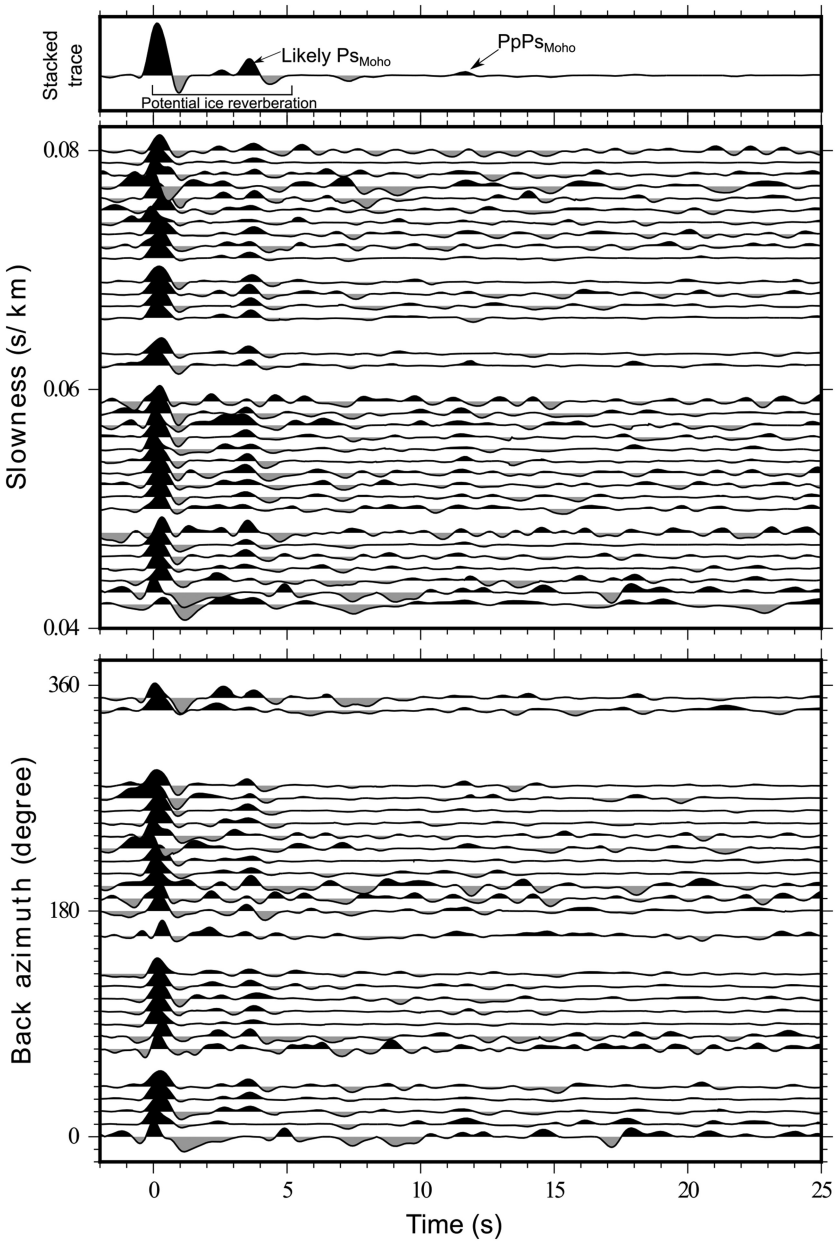

Figure 2. 2 Hz maximum frequency radial receiver functions recorded from 2016 to 2018 at station PIG1 (Fig. 1) binned by backazimuth every 10° and slowness every 0.001 s km^{-1}. A stacked trace containing 134 individual receiver functions after quality control is displayed above. PIG1 has 1.2 km of underlying ice (Fretwell *et al.* 2013), as a result the relative signal contribution in the first 6 s from the crustal Ps_{Moho} phase and ice reverberation is difficult to constrain.

(Ps_{ice}) and reverberations ($PpPs_{ice}$) introduced by the addition of a subglacial sediment layer.

To obtain 95 per cent confidence intervals for the grid search result we use a bootstrap resampling scheme (Fig. 3c). We produce 5000 randomly sampled receiver function stacks from the data and then compute the misfit with respect to the best-fitting synthetic receiver function produced by the forward modelling. Assuming a normal Gaussian distribution of misfit we then extract 95 per cent confidence limits. Subglacial sediment thickness is generally reasonably well constrained to within ±0.2 km, whilst sediment V_s is less so, varying from ±0.2 to ±1.0 km s^{-1} at different stations (see Table S1).

3.4 Joint inversion for crustal structure

Given that receiver functions are a time series, conversion of a time interval to depth requires knowledge of the corresponding velocity structure. Rayleigh wave phase velocity dispersion data is sensitive to average shear wave velocity structure, therefore it is often advantageous to use a joint inversion of Rayleigh wave dispersion curves and receiver functions when aiming to constrain crustal structure. To estimate crustal thickness and obtain a crustal shear wave velocity model at each station, we use the method of Julia *et al.* (2000) for jointly inverting receiver functions and Rayleigh wave phase velocity dispersion data. The method produces a layered

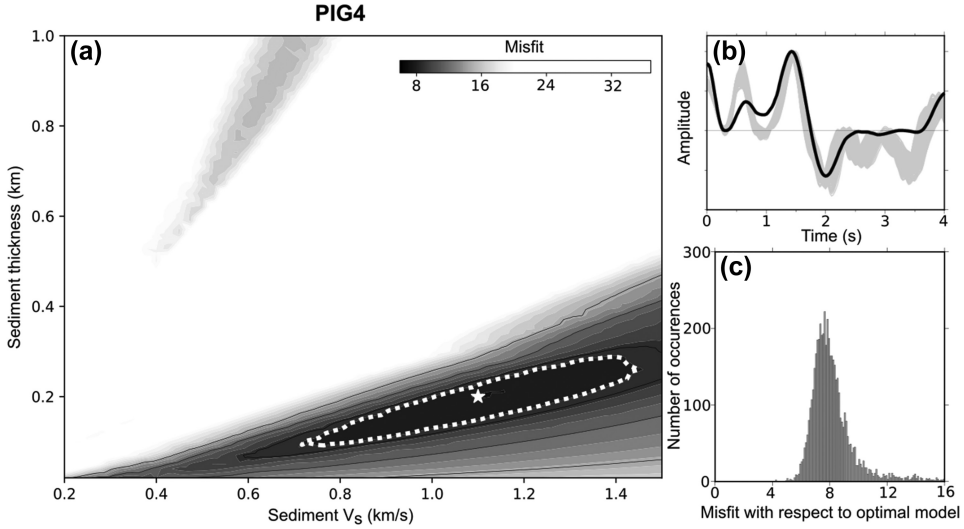

Figure 3. (a) Subglacial sediment forward modelling results for station PIG4 (Fig. 1). The best-fitting model is denoted by a white star, and 95 per cent confidence bounds are shown as dashed white line. (b) Best-fitting forward modelled receiver functions. The stacked receiver function is shown as a solid black line, and synthetic receiver functions from within the 95 per cent confidence bounds are shown in grey. (c) Bootstrap analysis to estimate uncertainty of subglacial sediment forward modelling following the method of Chaput *et al.* (2014). We produce 5000 bootstrapped receiver functions from the data and compute misfit with respect to the best-fitting models from part (a). Assuming the misfit has a normal Gaussian distribution we can then estimate 95 per cent confidence bounds.

shear velocity–depth profile by solving a linearized damped least-squares joint inversion. This inversion technique also allows for the inclusion of *a priori* information on layer depths and velocities.

In the initial model at each station the crust is parametrized as 2.5-km-thick layers with a gradually increasing shear wave velocity from 3.4 to 4.0 km s^{-1} and an overall crustal thickness of 35 km. The crust overlies a uniform upper mantle with a V_s of 4.5 km s^{-1}. At each station we include the best-fitting near surface subglacial sediment identified in the forward modelling, and ice thickness from BEDMAP2 (Fretwell *et al.* 2013). Including the ice layer in the initial model allows the additional complexity in the receiver function to be accounted for in the joint inversion process. A similar approach was taken by Shen *et al.* (2018), who find the incorporation of receiver functions provides additional constraints on crustal structure than inverting surface wave data alone. The subglacial sediment layer thickness is fixed, but V_s is allowed to change in the inversion process, as the absolute shear wave velocity is loosely constrained in the forward modelling step. Layer thickness is fixed at 2.5 km from the base of the ice/sediment to 50 km, and at 5 km from 50 to 80 km.

At each station we use a Rayleigh wave phase velocity dispersion curve in the 8–50 s period range modelled in the O'Donnell *et al.* (2019a, b) studies. The dispersion curves are constrained to within ±0.05 km s^{-1} at all periods. For more information on the generation of the Rayleigh wave phase velocity dispersion curves and the associated uncertainty please see O'Donnell *et al.* (2019a, b). We then jointly invert this with receiver functions stacked into narrow ray parameter bins of 0.040–0.049, 0.050–0.059, 0.060–0.069 and >0.070 s km^{-1} at two maximum frequencies, 0.5 and 2 Hz (Fig. 4). As described in Julia *et al.* (2000) we equalize the number of data points and physical units in both data sets, allowing us to give each equal weight in the joint inversion. The ±0.05 km s^{-1} uncertainty in the Rayleigh wave phase velocity dispersion data was included as part of the inversion process.

To evaluate uncertainty in the final V_s models arising from the stacked receiver functions, we use a bootstrapping procedure which involves repeating the inversion process 500 times each with randomly resampled receiver function stacks (e.g. Bao *et al.* 2015; Emry *et al.* 2015). Each bootstrap receiver function stack was produced by randomly selecting receiver functions from the data set with replacement and then stacking. To determine the corresponding uncertainty for our crustal thickness value, we inspect the bootstrap shear wave velocity limits of layers neighbouring the interpreted Moho from the full ensemble of bootstrap models. We find that the error in our velocity models is constrained to ±0.15 km s^{-1} and the Moho depth to ±2.5–5 km at most stations. These uncertainty constraints are comparable to other studies of crustal thickness in the region (e.g. Chaput *et al.* 2014; Ramirez *et al.* 2017). Additional uncertainty in the joint inversion results arises due to the V_p/V_s ratio remaining fixed in the inversion. After testing the joint inversion with a range of crustal V_p/V_s ratios (1.7–1.8), we find that the uncertainty arising from the V_p/Vs ratio is within the bootstrap error bounds, and the interpreted Moho would remain the same (see the Supporting Information).

3.5 Interpreting final shear wave velocity–depth models

The output from the joint inversion is a shear velocity–depth profile (Fig. 4), which requires interpretation to determine the crustal thickness at each station. We interpret the Moho in each final model to be the depth at which there is a >0.25 km s^{-1} shear wave velocity increase in the 4.0–4.3 km s^{-1} range, or when the shear wave velocity exceeds 4.3 km s^{-1} following Ramirez *et al.* (2017). As stated in Ramirez *et al.* (2017) lower crustal shear wave velocities derived from V_p/V_s ratios from experimental data (e.g. Holbrook *et al.* 1992; Christensen & Mooney 1995; Christensen 1996) rarely exceed 4.3 km s^{-1}. Shear wave velocities at or above 4.3 km s^{-1} are therefore more likely to represent upper mantle than crustal lithologies. Whilst a shear wave velocity of 4.3 km s^{-1} is not globally characteristic of the upper mantle, the expectation of an instantaneous jump in V_s to values exceeding 4.5 km s^{-1} as indicated by global velocity models may not always be reasonable. Lebedev *et al.*

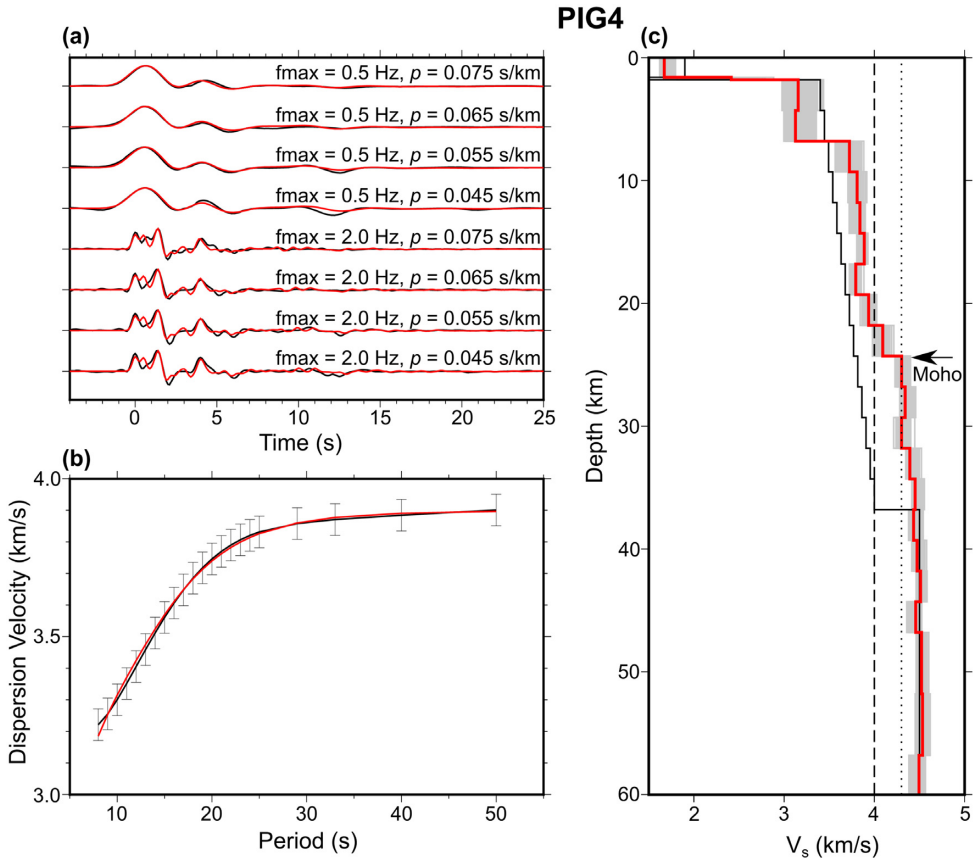

Figure 4. Joint inversion results from station PIG4. (a) Receiver functions with corresponding model results (red) stacked into narrow ray parameter (p) bins at two maximum frequencies (0.5 and 2 Hz). Stacked input receiver functions are in black and the resulting inverted receiver functions are in red. (b) Rayleigh wave phase velocity dispersion curve inversion results. The input Rayleigh wave phase velocity dispersion curve is in black and the inversion result in red, showing a good fit within the ±0.05 km s^{-1} uncertainty limits. (c) The shear wave velocity–depth profile produced by the joint inversion. The initial model is in black and the final V_s–depth profile produced by the inversion is shown in red. Models produced by 500 bootstrap iterations are displayed in grey solid lines, indicating that V_s is generally constrained to within ±0.15 km s^{-1}. Dashed and dotted lines are added at 4.0 and 4.3 km s^{-1}, respectively, to indicate the layers of likely mafic lower crust.

(2009) suggest that upper mantle velocities increase with depth from the Moho to a maximum before decreasing again due to the spinel peridotite-garnet peridotite transition. When interpreting the Moho we therefore seek a rapid increase or jump in shear wave velocity from likely crustal values to values exceeding 4.3 km s^{-1} range, rather than when 4.5 km s^{-1} is reached.

Our method for interpreting the Moho depth in the final shear wave velocity models follows other similar studies of crustal thickness in the same region (Ramirez *et al.* 2017; O'Donnell *et al.* 2019a). Despite this, a sharp jump from typical lower crustal to upper mantle shear wave velocities is not present at all stations. This is likely due to the Ps_{Moho} phase being masked by the reverberations from shallow low velocity structure, such as the ice layer, in the receiver function. Our modelled crustal thickness at stations where this is the case are therefore predominantly controlled by the Rayleigh Wave dispersion data, and have a higher associated uncertainty.

To further characterize the composition and nature of the crust at each station, we divide the crust into likely sedimentary, felsic/intermediate upper crust and mafic lower crustal layers based on the modelled shear wave velocity structure. Studies of crustal structure and composition (e.g. Rudnick & Fountain 1995) have suggested that felsic-to-intermediate crust tends to have a shear wave velocity of <3.9 km s^{-1}, whilst common lower crustal mafic lithologies tend to have shear wave velocity of >3.9 km s^{-1}. We suggest that crustal layers with a V_s <3.2 km s^{-1} likely represents sediments, V_s of 3.2–4.0 km s^{-1} represent likely felsic to intermediate crust, whilst a V_s of 4.0–4.3 km s^{-1} indicate likely mafic lower crust.

4 RESULTS

At each station we have produced models of crustal thickness and shear wave velocity structure (Fig. 5). The Antarctic Peninsula and HEW blocks host the thickest crust we interpret in this study, with crustal thickness ranges of 30–38 km and 30–40 km, respectively. In both these blocks we also find the largest relative abundance of likely felsic-to-intermediate crust with a V_s from 3.2 to 3.9 km s^{-1}. The thinnest crust we interpret is within the WARS, with a thickness range of 18–28 km. Within the WARS we also model the overall highest relative proportion of high velocity, likely mafic lower crust to likely felsic/intermediate crust (Fig. 5).

Within the HEW block we find the thickest crust at stations HOWD, WILS and UNGL, at 40, 38 and 38 ± 5 km, respectively. All three stations are located within the Ellsworth Mountain section of the block, whilst stations within the Whitmore Mountain and Haag Nunatak sections of the block feature a thinner crust at ∼33 km. Given that most stations within the HEW and Antarctic Peninsula

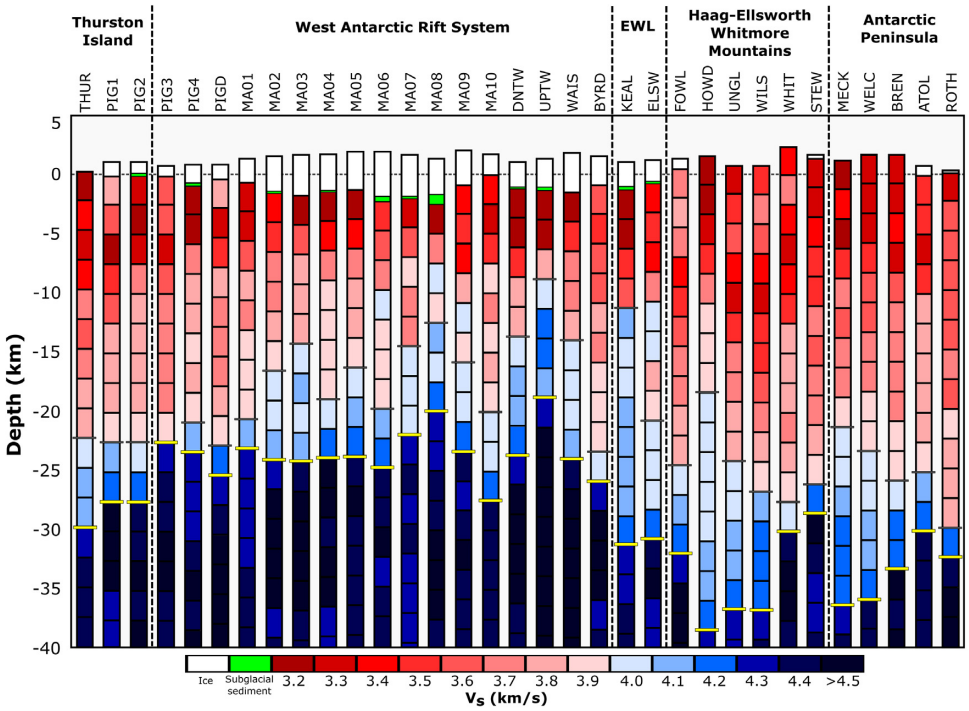

Figure 5. A summary of our V_s–depth profiles at each station, grouped by crustal block. We also group stations in the Ellsworth Land (EWL) region, given the ambiguity as to which block these stations belong. Each crustal column is coloured by modelled shear wave velocity, with red colours indicating likely felsic-to-intermediate crust and blue representing likely mafic lower crust. Upper mantle is displayed in dark blue, subglacial sediment in green and ice in white. Our interpreted transition from felsic/intermediate crust to mafic lower crust is indicated with a horizontal grey line at each station, and our interpreted Moho with a yellow line. We include the ice thickness from Fretwell *et al.* (2013) and the subglacial sediment thickness identified in the forward modelling stage.

are situated on the flanks of nunataks and on bedrock, no subglacial sediment was identified within these blocks.

Stations ELSW and KEAL are located close to the northern edge of the HEW block in Ellsworth Land, and feature fundamentally different crust to that seen within the interior of the HEW. We observe a shallower Moho at 30 ± 2.5 km with a seemingly two layer crust. A slow upper crust of ∼3.4 km s^{-1} overlies a fast and relatively uniform middle and lower crust with an average V_s of 4.0 km s^{-1}. The internal crustal structure at these stations is similar to those in the centre of the WARS, however both feature a deeper Moho. Additionally we identify subglacial sediment at both stations with a thickness of 0.1–0.2 km and V_s of ∼1.0 km s^{-1}.

In the centre of the WARS we find slow upper crustal layers V_s <3.2 km s^{-1}, underlain by 10–15 km of likely felsic crust and a 5–10-km-thick likely mafic lower crust with a V_s >4.0 km s^{-1}. The thinnest crust imaged in this study at 18–20 km come from stations MA07, MA08 and UPTW, all of which lie in the vicinity of either the Byrd Subglacial Basin or Bentley Subglacial Trench.

Subglacial low velocity sediment identified in the forward modelling is present at 10 stations within the WARS and Thurston Island and Ellsworth Land with a range of thicknesses from 0.1 to 0.8 km. Shear wave velocity in these layers varies from 0.4 to 1.6 km s^{-1} (see the Supporting Information). At stations MA09 and MA10 our best-fitting model features a 0.1–0.3-km-thick subglacial layer with a V_s of ∼1.9 km s^{-1} which is close to that of ice (Kohnen 1974), indicating that at these stations there may be thicker ice than indicated by BEDMAP2. At station UPTW we use the subglacial sediment thickness and V_s from Chaput *et al.* (2014) to parametrize the initial model, as our forward modelling did not produce a stable solution at this station.

5 DISCUSSION

To build on our current knowledge of West Antarctica's crustal framework, we consider our estimates of crustal thickness and shear wave velocity structure in the context of the regional tectonics. Improving our grasp on West Antarctica's tectonic framework is essential for building a comprehensive understanding of the region's evolution. By inspecting the broad crustal structure of each crustal block, we can contrast West Antarctica's tectonic mosaic with analogous regions worldwide.

Our crustal thickness estimates from West Antarctica are compatible with other seismic and gravity studies conducted in the region, as summarized in Table 1. In the WARS our crustal thickness range of 18–28 km is in good agreement with seismic (Winberry & Anandakrishnan 2004; Baranov & Morelli 2013; Chaput *et al.* 2014; Ramirez *et al.* 2016; Shen *et al.* 2018) and gravity derived crustal thickness estimates (Jordan *et al.* 2010; O'Donnell & Nyblade 2014). Stations BYRD, DNTW, UPTW and WAIS are featured in previous receiver function (Chaput *et al.* 2014) and *S*-wave receiver function (Ramirez *et al.* 2016) studies. Our crustal thickness estimates agree within uncertainty bounds with Chaput *et al.* (2014) at all four stations, but we find 10-km-thinner crust at UPTW than Ramirez *et al.* (2016).

5.1 Tectonic interpretation of V_s profiles

Fig. 6 shows our crustal thickness estimates plotted alongside the ambient seismic noise derived crustal thickness model of O'Donnell *et al.* (2019a). Given the similar input dispersion data sets we see a good general agreement between crustal thickness estimates (see

Table 1. Crustal thickness estimates from present and previous studies.

	Crustal thickness range (km)		
Crustal block	This study	Other studies	Reference
West Antarctic Rift System	18–28	21–31	Winberry & Anandakrishnan (2004)
		20–25	Jordan *et al.* (2010)
		20–28	Baranov & Morelli (2013) and references therein
		25–28	O'Donnell & Nyblade (2014)
		21–28	Chaput *et al.* (2014)
		19–29	Ramirez *et al.* (2016)
		20–30	Shen *et al.* (2018)
Thurston Island	28–30	24–26	Jordan *et al.* (2010)
		24–28	Baranov & Morelli (2013) and references therein
		∼25	O'Donnell & Nyblade (2014)
		28–35	Shen *et al.* (2018)
Haag-Ellsworth Whitmore	30–40	30–40	Baranov & Morelli (2013) and references therein
		28–36	O'Donnell & Nyblade (2014)
		30–37	Chaput *et al.* (2014)
		35–38	Ramirez *et al.* (2017)
		30–43	Shen *et al.* (2018)
Antarctic Peninsula	30–38	34–44	Baranov & Morelli (2013) and references therein
		29–34	O'Donnell & Nyblade (2014)

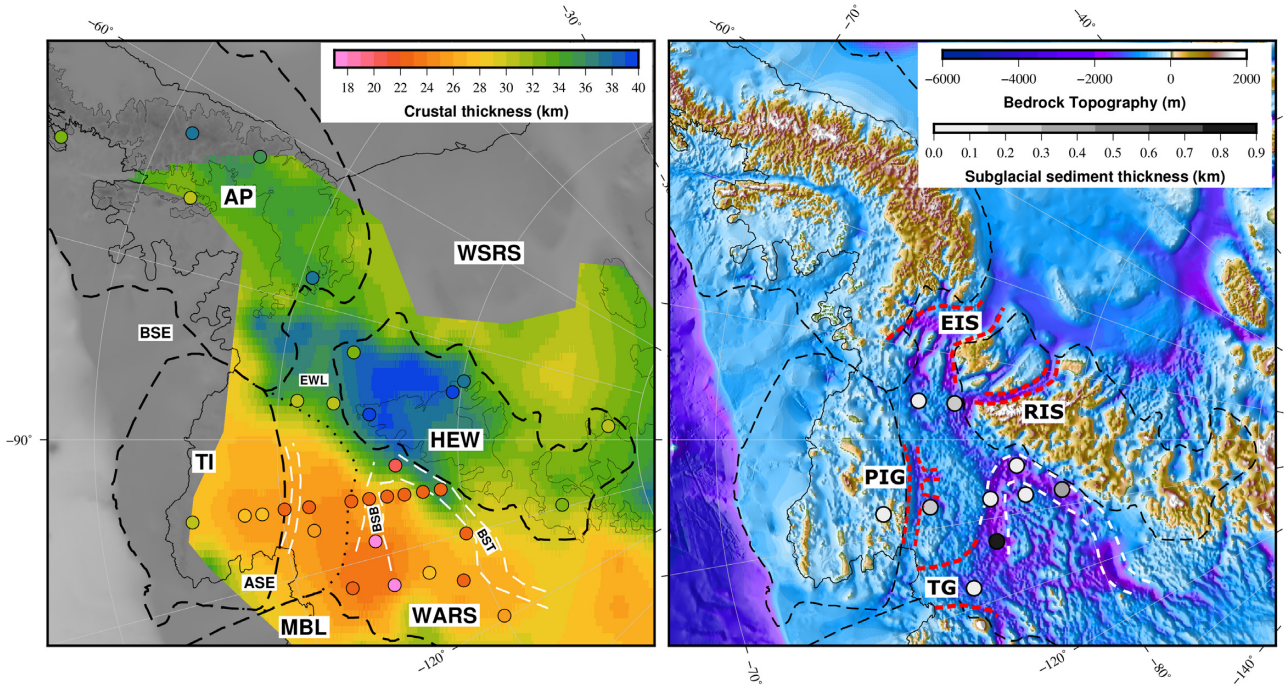

Figure 6. Left-hand panel: a map of our crustal thickness estimates at each station (circles) superimposed on the ambient noise derived crustal thickness map of O'Donnell *et al.* (2019a). The crustal block boundaries of Dalziel & Elliot (1982) are in dashed black except for the Thurston Island-WARS boundary which is dotted, here we have redrawn the Thurston Island-WARS boundary to encompass the thinner crust we have imaged at stations PIG3, PIG4 and MA01. Right-hand panel: a map of stations at which we infer subglacial sediment from forward modelling, coloured by layer thickness over BEDMAP2 bedrock topography. All subglacial sediment that we identify in this study lies in the WARS and Ellsworth Land, predominately at stations in the vicinity of the Byrd Subglacial Basin and Bentley Subglacial Trench. Major ice streams roughly outlined in red dashed are the following: Evans Ice Stream (EIS), Rutford Ice Stream (RIS), Pine Island Glacier (PIG) and Thwaites Glacier (TG).

Table S1), however the inclusion of receiver functions in this study improves resolution of crustal structure and discontinuities at each station. Our minimum crustal thickness comes from the Byrd Subglacial Basin, and is ∼5 km thinner than that of O'Donnell *et al.* (2019a). Given that the spatial resolution of the ambient noise crustal model of O'Donnell *et al.* (2019a) is on the order of ∼300 km it is likely that these narrow rifts are not fully resolved. As such, the combination of both the crustal thickness model of O'Donnell *et al.* (2019a) and the joint inversion results from this study can provide an enhanced image of West Antarctica's crustal mosaic.

We find the thinnest crust in this study in the centre of the WARS; an area which also hosts the Byrd Subglacial Basin and Bentley Subglacial Trench. In addition in this area we find the highest proportion of fast, likely mafic lower crust as shown by Fig. 5. The isostatic impact of the potentially high relative abundance of dense mafic crust may be a contributing factor in the region's extremely low observed

bedrock elevation (Fretwell *et al.* 2013), in combination with the isostatic adjustment of the thick ice overburden. We model a thinner crust and higher proportion of mafic lower crust in comparison to the Mesozoic/Cenozoic extensional type section of Rudnick & Fountain (1995); our WARS models are more in line with the active rifts that Rudnick & Fountain (1995) analyse. We therefore suggest that the thin crust with a thick mafic lower crustal layer we model in the vicinity of the Byrd Subglacial Basin and Bentley Subglacial Trench is supportive of additional Neogene rifting impacting the central and eastern WARS (e.g. Jordan *et al.* 2010). A comparable rift system to the WARS in terms of scale (but not elevation) is the Cenozoic Basin and Range province, which features crust ranging from 30 to 35 km thick (Zandt *et al.* 1995). The thinner WARS crust supports the suggestion that it has undergone enhanced localized thinning relative to the Basin and Range. The highly mafic lower crust we model, in combination with the localized deep subglacial basins of the Byrd Subglacial Basin and Bentley Subglacial Trench, is comparable to the southern section of the Kenya Rift Zone and Baikal Rift Zone (Thybo & Artemieva 2013). In these regions the presence of mafic underplating and sills in the lower crust has lead to magma compensated crustal thinning, and a deep rift graben forming above.

Within the Antarctic Peninsula we find an average crustal thickness of 35 km with ∼75 per cent of the crust being composed of lower velocity likely felsic to intermediate material (Fig. 5). As such, the crustal thickness and velocity structure that we see in the Antarctic Peninsula is consistent with an arc tectonic environment (e.g. Christensen & Mooney 1995). Models of subglacial heat flux on the Antarctic Peninsula have suggested that the southern and eastern sections of the Peninsula have a high flux, up to 100 mWm^{-2} in places (Burton-Johnson *et al.* 2017). Areas of elevated heat flux on the Antarctic Peninsula coincide with UKANET stations ATOL, BREN and WELC, all of which show relatively slow upper and mid crustal average shear wave velocities and a thin mafic lower crust with respect to the total crustal thickness (Fig. 5). A predominantly felsic to intermediate crustal composition in this region would provide capacity for high radiogenic heat production as suggested by Burton-Johnson *et al.* (2017).

We find along strike variability in crustal thickness within the HEW block, from the Haag Nunatak section through the Ellsworth Mountains and into the Whitmore Mountains. We find the thickest crust in this study in the Ellsworth Mountain section of the HEW block at 38–40 km at stations HOWD, UNGL and WILS. Stations within the Whitmore Mountain section of the HEW block image a thinner (30–33 km), and more felsic-like crust than the Ellsworth Mountain section of the block (Fig. 5). This spatial variability of crustal thickness and structure within the HEW block has previously been noted by other seismic and aerogravity studies (Jordan *et al.* 2010; Chaput *et al.* 2014; Heeszel *et al.* 2016; Ramirez *et al.* 2017; O'Donnell *et al.* 2019a). The UKANET station FOWL is the first to be deployed in the Haag Nunatak section of the HEW block, and here we infer ∼7.5 km thinner crust (33 ± 2.5 km), and a contrasting crustal structure to the neighbouring POLENET/ANET stations in the Ellsworth Mountains (HOWD, UNGL and WILS). The fast upper crust we infer at FOWL may be indicative of additional potentially mafic intrusions in the upper crust relative to surrounding stations in Ellsworth Land and the HEW. The basement exposure of the Haag Nunataks is among the oldest sampled in West Antarctica at ∼1 Ga (Millar & Pankhurst 1987), and the crustal thickness we model is ∼10 km thinner than the characteristic seismically imaged Proterozoic crust of Durrheim & Mooney (1991). The Proterozoic crust studied in Durrheim & Mooney (1991) also includes a thick high velocity layer at the base of the crust which is attributed to basaltic underplating, and at FOWL we infer a 7.5-km-thick likely mafic lower crust. A possible explanation for the reduced crustal thickness we model at FOWL relative to other characteristic Proterozoic crust is through lower crustal flow into neighbouring tectonic blocks. Lower crustal flow from the Haag Nunataks into the Weddell Sea Rift System in the Jurassic has previously been proposed by Jordan *et al.* (2017), which would have acted to enhance Weddell Sea Rift System extension.

5.2 Refining the bounds of the WARS

According to the crustal block boundaries of Dalziel & Elliot (1982), the tectonic block in which UKANET stations ELSW and KEAL are situated is indeterminate. This region is crucial for revealing any possible connectivity with the Weddell Sea Rift System. The overall crustal thickness at the Ellsworth Land stations (30 ± 5 km) is comparable to the neighbouring Haag Nunataks, yet the internal crustal structure features a thicker (10–20 km thick) high-velocity likely mafic lower crust. As previously noted, the potential abundance of dense mafic lower crust may be responsible for the deep bedrock elevations in the region, whilst the overall thicker crust suggests that Ellsworth Land has undergone less extension than the central WARS. The presence of extensive mafic underplating in the neighbouring Weddell Sea Rift System has been attributed to plume related Jurassic magmatism by Jordan *et al.* (2017); a similar mechanism may have been responsible for the thick mafic lower crust which we model in Ellsworth Land. An alternative interpretation is that lower crustal flow from the Haag Nunataks transferred mafic material not only to the Weddell Sea Rift System but also into Ellsworth Land. Were this to be the case then a lateral pressure gradient in the lower crust would have to have been present to facilitate upper crustal extension, suggesting that the region has been subject to some stretching. The disparity in both crustal thickness and structure with regards to the central WARS suggests that the rift system did not substantially propagate into Ellsworth Land. We therefore suggest that there is not a direct linkage between the WARS and Weddell Sea Rift System, and that the WARS instead propagated in the direction of the Bellingshausen and Amundsen Sea embayments.

The UKANET-POLENET Mini Array traverse (PIG1-MA06) crosses from Thurston Island into the WARS, and as such can be utilized to better constrain the northern boundary of the WARS. Fig. 7 shows the shear wave velocity–depth profiles from the Pine Island Glacier station traverse. At stations in the centre of the WARS (PIG3-MA05) we find crust with a consistent thickness of 23–25 km, whilst at Thurston Island stations (THUR-PIG2) we find a thicker crust of 28–30 km. Our findings therefore support the suggestion that the WARS-Thurston Island block boundary lies in the vicinity of the Pine Island Rift. A number of previous studies have proposed that the Pine Island Rift is a branch of the WARS (Gohl *et al.* 2007; Jordan *et al.* 2010; Gohl 2012; Damiani *et al.* 2014), and that the region between the Pine Island Rift and the Byrd Subglacial Basin is a transitional crustal boundary zone (Diehl 2008). The gradual decrease in crustal thickness that we model from PIG2 to MA01 is supportive of this region being a transitional area from Thurston Island to WARS crust. The transition from WARS to Thurston Island crust is more subtle than on the opposing flank of the rift system. The sharp change in crustal character and bedrock elevation between the WARS and HEW block suggests that this

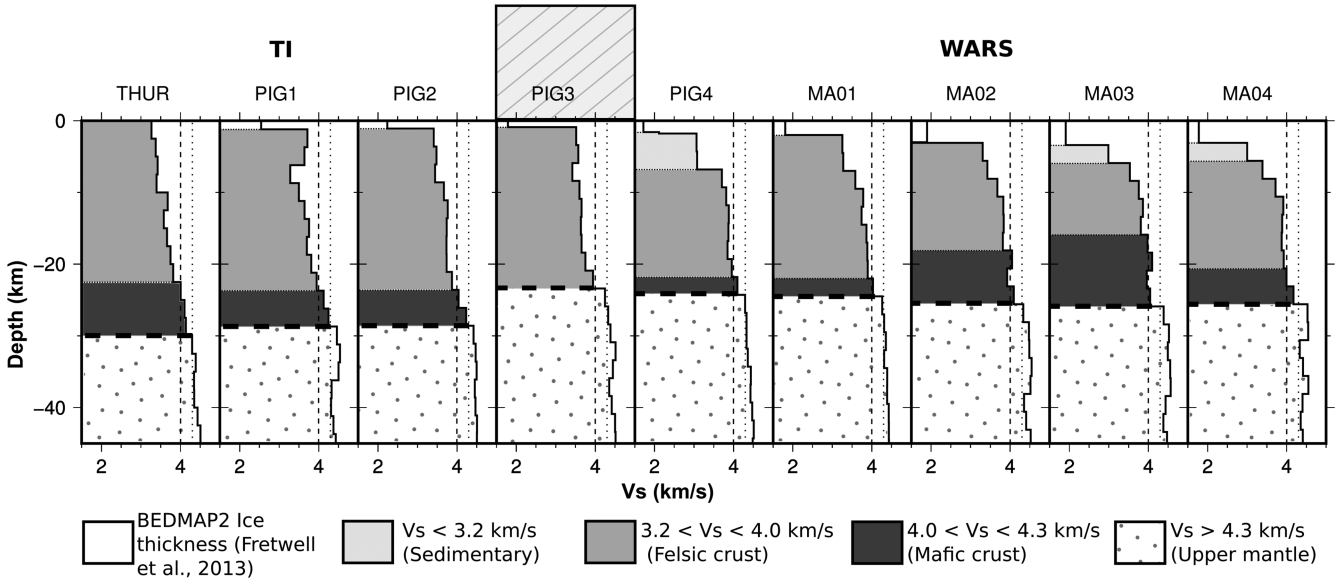

Figure 7. Shear wave velocity structure from the UKANET-POLENET/ANET Mini Array traverse stations which sample the transition from the Thurston Island (TI) block into the WARS. Our interpreted Moho is shown by a horizontal dashed black line at each station, and we add vertical dashed and dotted lines at 4.0 and 4.3 km s^{-1}, respectively to indicate the transition from lower crustal to upper mantle velocities. We interpret the Thurston Island-WARS transition to lie in the vicinity of PIG3 as shown by the dashed box. Within Thurston Island we find a ∼28-km-thick crust, whilst in the WARS we find a 3−5-km-thinner crust with a higher proportion of fast (4.0–4.3 km s^{-1}) lower crust.

boundary may instead be more fault controlled than the Thurston Island-WARS flank.

Gohl (2012) and Bingham *et al.* (2012) both suggest that major ice streams in West Antarctica exploit tectonic lineaments created by rifting. Our estimates of crustal thickness support the suggestion that Pine Island Glacier could be steered by WARS rift structures. Were the Thurston Island-WARS boundary to be in the vicinity of the Pine Island Rift then that would imply a ∼200 km shift from its previously accepted position in Dalziel & Elliot (1982). If the WARS is indeed 200 km wider, then there are implications for modelling plate circuit closure and for the total amount of extension encompassed by the WARS. The new boundary we propose also suggests that the WARS extends further towards both the Amundsen Sea and Bellingshausen Sea embayments than previously thought (Fig. 6).

5.3 Estimating subglacial sediment thickness

Fig. 6 features a map of all stations at which we identify low velocity subglacial layers in the forward modelling. Subglacial layers of this thickness (0.1–0.8 km) and shear wave velocity (0.4–1.6 km s^{-1}) are indicative of unlithified, soft and possibly saturated sediment (Winberry & Anandakrishnan 2004). We find low velocity subglacial layers at 10 stations within the WARS, Thurston Island and Ellsworth Land, with the majority at stations in the vicinity of the Byrd Subglacial Basin and Bentley Subglacial Trench. These deep subglacial basins could provide ample accommodation space for the accumulation of relatively thick subglacial sediment, which in turn may have provided the basal till to accelerate regional ice flow. The abundance of soft unlithified sediment in the central portion of the WARS could well have been a contributing factor for the fast flow observed in the Thwaites Glacier region (Rignot *et al.* 2011). Soft deforming till layers have been identified in the upper reaches of Thwaites Glacier using seismic reflection (Muto *et al.* 2019), much of which may have been sourced from the thick subglacial sediment accumulations we model in the Byrd Subglacial Basin. Subglacial sediment has also been identified within the deep basins of the central WARS by Pourpoint *et al.* (2019), who used a joint inversion of receiver functions, Rayleigh and Love dispersion, and Rayleigh wave horizontal-to-vertical amplitude ratio. Pourpoint *et al.* (2019) modelled sediment to be 1.5 km thick beneath station MA08, and >0.5 km thick at stations DNTW, UPTW, MA06 and MA07.

In addition we find 0.1–0.2-km-thick subglacial sediment present in the vicinity of Pine Island Glacier at PIG2 and PIG4, another region of fast ice flow. Large-scale sedimentary deposits have previously been identified using seismic reflection (Brisbourne *et al.* 2017), and aerogravity models indicate there could be ∼0.8-km-thick sediments near the glacier's grounding line (Muto *et al.* 2016).

Another region in which we infer the presence of low velocity subglacial sediment is at stations ELSW and KEAL (Fig. 6), both of which lie upstream of the Rutford Ice Stream and Evans Ice Stream. The Rutford Ice Stream flows at a velocity up to ∼400 m a^{-1} (Gudmundsson 2006), yet it has a gentle surface slope relative to other fast flowing West Antarctic ice streams suggesting that the basal driving stress is low (e.g. MacAyeal *et al.* 1995). To accommodate such a high velocity with a low basal driving stress the basal friction must also be low, implying that soft sediment must be present. A number of studies have confirmed the presence of large scale sedimentary bedforms beneath the Rutford Ice Stream, using both seismic surveying and ice penetrating radar (King *et al.* 2007; Smith & Murray 2009). In the Evans Ice Stream, Vaughan *et al.* (2003) measured acoustic impedance to reveal that the entire bed of the ice stream consists of dilated sediment. The 0.1–0.3-km-thick low velocity sedimentary layer that we model at ELSW and KEAL could have provided an upstream source for the subglacial sediments identified beneath the Rutford Ice Stream and Evans Ice Stream, which has subsequently acted to accelerate flow.

6 CONCLUSIONS

Through a joint inversion of receiver functions and Rayleigh wave phase velocity dispersion data, we image crustal shear velocity structure at 33 seismic stations across West Antarctica. The thinnest surveyed crust in our study lies within the WARS (18–28 km), bounded by thicker crust in the neighbouring Haag-Ellsworth Whitmore (30–40 km), Antarctic Peninsula (30–38 km) and Thurston Island (28–30 km) blocks. We find the highest relative proportion of likely mafic lower crust to potential felsic/intermediate crust in the WARS, and especially in the neighbouring Ellsworth Land. By contrasting the crustal structure at Thurston Island and the WARS, we suggest that the boundary between the two blocks lies in the vicinity of the Pine Island Rift, ∼200 km north of its previously inferred position from Dalziel & Elliot (1982). In addition, from high frequency receiver functions we infer that 0.1–0.8-km-thick low seismic velocity subglacial sediment is present beneath 10 stations within the WARS, Thurston Island and Ellsworth Land. Thick subglacial sediment accumulations of this type could have acted as a source for the soft sediment layers identified beneath many fast flowing West Antarctic ice streams, reducing basal friction.

ACKNOWLEDGEMENTS

We would like to thank both reviewers and the editor for their constructive comments on our manuscript. We thank all BAS camp staff, field guides and air unit personnel for the logistical support of the UKANET seismic and GNSS networks. We similarly acknowledge all academic members, field teams and camp staff associated with the POLENET/ANET project and thank Kenn Borek Air and the New York Air Guard for flight support. CKD and JPOD are supported by the Natural Environment Research Council [grant NE/L006065/1]. POLENET/ANET is supported by the National Science Foundation Office of Polar Programs [grants 0632230, 0632239, 0652322, 0632335, 0632136, 0632209, and 0632185]. UKANET seismic instrumentation was provided and supported by SEIS-UK. POLENET/ANET seismic instrumentation was provided and supported by the Incorporated Research Institutions for Seismology (IRIS) through the PASSCAL Instrument Center. The UKANET (www.ukanet.wixsite.com/ukanet; network code 1D; https://doi.org/10.7914/SN/1D_2016) data will be accessible through the IRIS Data Management Center (http://www.iris.edu/mda) from January 2021. POLENET/ANET (network code YT), seismic data can be accessed through the IRIS DMC. The facilities of the IRIS Consortium are supported by the NSF under cooperative agreement EAR1063471, the NSF Office of Polar Programs, and the DOE National Nuclear Security Administration. We would also like to thank Joe Cann for helpful comments on the paper. Figures were created using the Generic Mapping Tools (GMT) software (Wessel & Smith 1998).

REFERENCES

Anandakrishnan, S. & Winberry, J.P., 2004. Antarctic subglacial sedimentary layer thickness from receiver function analysis, *Global Planet. Change,* **42,** 167–176.

Anthony, R.E., *et al.*, 2015. The seismic noise environment of Antarctica, *Seismol. Res. Lett.,* **86**(1), 89–100.

Bao, X., *et al.*, 2015. Two crustal low-velocity channels beneath SE Tibet revealed by joint inversion of Rayleigh wave dispersion and receiver functions, *Earth planet. Sci. Lett.,* **415,** 16–24.

Baranov, A. & Morelli, A., 2013. The Moho depth map of the Antarctica region, *Tectonophysics,* **609,** 299–313.

Barletta, V.R., *et al.*, 2018. Observed rapid bedrock uplift in Amundsen Sea Embayment promotes ice-sheet stability, *Science,* **360**(6395), 1335–1339.

Behrendt, J.C., 1999. Crustal and lithospheric structure of the west Antarctic Rift System from geophysical investigations—a review, *Global Planet. Change,* **23**(1–4), 25–44.

Behrendt, J.C. & Cooper, A., 1991. Evidence of rapid Cenozoic uplift of the shoulder escarpment of the Cenozoic west antarctic rift system and a speculation on possible climate forcing, *Geology,* **19**(4), 315–319.

Behrendt, J.C., LeMasurier, W.E., Cooper, A.K., Tessensohn, F., Tréhu, A. & Damaske, D., 1991. Geophysical studies of the West Antarctic Rift System, *Tectonics,* **10**(6), 1257.

Bingham, R.G., Ferraccioli, F., King, E.C., Larter, R.D., Pritchard, H.D., Smith, A.M. & Vaughan, D.G., 2012. Inland thinning of west antarctic ice sheet steered along subglacial rifts, *Nature,* **487**(7408), 468.

Birkenmajer, K., Delitala, M., Narebski, W., Nicoletti, M. & Petrucciani, C., 1986. Geochronology of tertiary island-arc volcanics and glacigenic deposits, King George island, South Shetland islands (West Antarctica), *Bull. Polish Acad. Sci. Earth Sci.,* **34**(3), 257–273.

Blankenship, D., *et al.*, 2001. Geologic controls on the initiation of rapid basal motion for west antarctic ice streams: a geophysical perspective including new airborne radar sounding and laser altimetry results, in *The West Antarctic Ice Sheet: Behavior and Environment,* pp. 105–121, Wiley, doi:10.1029/AR077p0105.

Block, A.E., Bell, R.E. & Studinger, M., 2009. Antarctic crustal thickness from satellite gravity: implications for the Transantarctic and Gamburtsev Subglacial Mountains, *Earth planet. Sci. Lett.,* **288**(1–2), 194–203.

Brisbourne, A.M., *et al.*, 2017. Bed conditions of Pine Island Glacier, West Antarctica, *J. geophys. Res.,* **122**(1), 419–433.

Brocher, T.M., 2005. Empirical relations between elastic wavespeeds and density in the earth's crust, *Bull. seism. Soc. Am.,* **95**(6), 2081–2092.

Burton-Johnson, A., Halpin, J., Whittaker, J.M., Graham, F.S. & Watson, S.J., 2017. A new heat flux model for the antarctic peninsula incorporating spatially variable upper crustal radiogenic heat production, *Geophys. Res. Lett.,* **44**(11), 5436–5446.

Chaput, J., *et al.*, 2014. The crustal thickness of West Antarctica, *J. geophys. Res.,* **119,** 378–395.

Christensen, N.I., 1996. Poisson's ratio and crustal seismology, *J. geophys. Res.,* **101**(B2), 3139–3156.

Christensen, N.I. & Mooney, W.D., 1995. Seismic velocity structure and composition of the continental crust: a global view, *J. geophys. Res.,* **100**(B6), 9761–9788.

Dalziel, I.W., 1992. Antarctica: a tale of two supercontinents? *Ann. Rev. Earth planet. Sci.,* **20**(1), 501–526.

Dalziel, I.W.D. & Elliot, D.H., 1982. West Antarctica: problem child of Gondwanaland, *Tectonics,* **1**(1), 3.

Damiani, T.M., Jordan, T.A., Ferraccioli, F., Young, D.A. & Blankenship, D.D., 2014. Variable crustal thickness beneath Thwaites glacier revealed from airborne gravimetry, possible implications for geothermal heat flux in West Antarctica, *Earth planet. Sci. Lett.,* **407,** 109–122.

Diehl, T.M., 2008. *Gravity Analyses for the Crustal Structure and Subglacial Geology of West Antarctica, Particularly beneath Thwaites Glacier,* The University of Texas at Austin.

DiVenere, V.J., Kent, D.V. & Dalziel, I., 1994. Mid-cretaceous paleomagnetic results from Marie Byrd land, West Antarctica: a test of post-100 ma relative motion between East and West Antarctica, *J. geophys. Res.,* **99**(B8), 15 115–15 139.

Donnellan, A. & Luyendyk, B.P., 2004. Gps evidence for a coherent antarctic plate and for postglacial rebound in Marie Byrd land, *Global Planet. Change,* **42**(1), 305–311.

Durrheim, R.J. & Mooney, W.D., 1991. Archean and Proterozoic crustal evolution: evidence from crustal seismology, *Geology,* **19**(6), 606–609.

Eagles, G., Larter, R.D., Gohl, K. & Vaughan, A.P.M., 2009. West Antarctic Rift System in the Antarctic Peninsula, *Geophys. Res. Lett.,* **36,** 4–7.

Emry, E.L., Nyblade, A.A., Julia, J., Anandakrishanan, S., Aster, R.C., Wiens, D.A., Huerta, A.D. & Wilson, T.J., 2015. The mantle transition zone beneath West Antarctica: seismic evidence for hydration and thermal upwellings, *Geochem. Geophys. Geosyst.,* **16**(1), 40–58.

Fitzgerald, P., 2002. Tectonics and landscape evolution of the Antarctic plate since the breakup of Gondwana, with an emphasis on the West Antarctic Rift System and the Transantarctic mountains, *R. Soc. N. Zeal. Bull.,* **35,** 453–469.

Fretwell, P., *et al.*, 2013. Bedmap2: Improved ice bed, surface and thickness datasets for Antarctica, *Cryosphere,* **7**(1), 375–393.

Gohl, K., 2012. Basement control on past ice sheet dynamics in the Amundsen Sea Embayment, West Antarctica, *Palaeogeogr., Palaeoclimatol., Palaeoecol.,* **335,** 35–41.

Gohl, K., *et al.*, 2007. Geophysical survey reveals tectonic structures in the Amundsen Sea Embayment, West Antarctica, US Geological Survey Open-File Report, 2007-1047{http://pubs.usgs.gov/of/2007/1047/srp/srp047/}.

Gohl, K., Kalberg, T., Eagles, G., Dziadek, R., Kaul, N., Spiegel, C. & Lindow, J., 2015. The extent of the West Antarctic Rift System in the Amundsen Sea and Bellingshausen Sea sectors, *Proceedings of the XII International Symposium on Antarctic Earth Sciences (ISAES),* Goa, India, 13 July 2015–17 July 2015.

Granot, R., Cande, S.C., Stock, J.M. & Damaske, D., 2013. Revised Eocene-Oligocene kinematics for the West Antarctic rift system, *Geophys. Res. Lett.,* **40,** 1–6.

Grunow, M., Kent, D.V. & Dalziel, I.W.D., 1991. New paleomagnetic data from Thurston Island: implications for the tectonics of West Antarctica and Weddell Sea opening, *J. geophys. Res.,* **96**(B11), 17935.

Gudmundsson, G.H., 2006. Fortnightly variations in the flow velocity of Rutford Ice Stream, West Antarctica, *Nature,* **444**(7122), 1063.

Harry, D.L., Anoka, J.L. & Jha, S., 2018. Geodynamic models of the West Antarctic rift system: implications for the mantle thermal state, *Geosphere,* **14**(6), 2407–2429.

Heeszel, D.S., *et al.*, 2016. Upper mantle structure of central and West Antarctica from array analysis of Rayleigh wave phase velocities, *J. geophys. Res.,* **121**(3), 1758–1775.

Helffrich, G., 2006. Extended-time multitaper frequency domain cross-correlation receiver-function estimation, *Bull. seism. Soc. Am.,* **96**(1), 344–347.

Holbrook, W.S., Mooney, W.D. & Christensen, N.I., 1992. The seismic velocity structure of the deep continental crust, *Continental lower crust,* **23,** 1–43.

Jordan, T., Ferraccioli, F., Vaughan, D., Holt, J., Corr, H., Blankenship, D. & Diehl, T., 2010. Aerogravity evidence for major crustal thinning under the pine island glacier region (West Antarctica), *GSA Bull.,* **122**(5–6), 714–726.

Jordan, T., Ferraccioli, F. & Leat, P., 2017. New geophysical compilations link crustal block motion to Jurassic extension and strike-slip faulting in the Weddell Sea rift system of West Antarctica, *Gondwana Res.,* **42,** 29–48.

Julia, J., Ammon, C., Herrmann, R. & Correig, A.M., 2000. Joint inversion of receiver function and surface wave dispersion observations, *Geophys. J. Int.,* **143**(1), 99–112.

Kalberg, T., Gohl, K., Eagles, G. & Spiegel, C., 2015. Rift processes and crustal structure of the Amundsen Sea Embayment, West Antarctica, from 3D potential field modelling, *Mar. Geophys. Res.,* **36**(4), 263–279.

Kennett, B. & Engdahl, E., 1991. Traveltimes for global earthquake location and phase identification, *Geophys. J. Int.,* **105**(2), 429–465.

King, E.C., Woodward, J. & Smith, A.M., 2007. Seismic and radar observations of subglacial bed forms beneath the onset zone of Rutford ice stream, Antarctica, *J. Glaciol.,* **53**(183), 665–672.

Kohnen, H., 1974. The temperature dependence of seismic waves, *J. Glaciol.,* **13**(67), 144–147.

Langston, C.A., 1979. Structure under Mount Rainier, Washington, inferred from teleseismic body waves, *J. geophys. Res.,* **84**(B9), 4749.

Lebedev, S., Boonen, J. & Trampert, J., 2009. Seismic structure of Precambrian lithosphere: new constraints from broad-band surface-wave dispersion, *Lithos,* **109**(1–2), 96–111.

Lloyd, A.J., *et al.*, 2015. A seismic transect across West Antarctica: evidence for mantle thermal anomalies beneath the Bentley Subglacial Trench and the Marie Byrd Land Dome, *J. geophys. Res.,* **120**(12), 8439–8460.

Llubes, M., Florsch, N., Legresy, B., Lemoine, J.M., Loyer, S., Crossley, D. & Rémy, F., 2003. Crustal thickness in Antarctica from CHAMP gravimetry, *Earth planet. Sci. Lett.,* **212**(1–2), 103–117.

Lodge, A. & Helffrich, G., 2009. Grid search inversion of teleseismic receiver functions, *Geophys. J. Int.,* **178**(1), 513–523.

Luyendyk, B.P., 1995. Hypothesis for Cretaceous rifting of east Gondwana caused by subducted slab capture, *Geology,* **23**(4), 373–376.

MacAyeal, D.R., Bindschadler, R.A. & Scambos, T.A., 1995. Basal friction of ice streame, West Antarctica, *J. Glaciol.,* **41**(138), 247–262.

Machado, A., Chemale, F., Conceição, R.V., Kawaskita, K., Morata, D., Oteíza, O. & Van Schmus, W.R., 2005. Modeling of subduction components in the genesis of the Meso-Cenozoic igneous rocks from the south shetland arc, antarctica, *Lithos,* **82**(3), 435–453.

Millar, I. & Pankhurst, R., 1987. Rb-Sr geochronology of the region between the Antarctic Peninsula and the Transantarctic Mountains: Haag Nunataks and Mesozoic Granitoids, in *Gondwana Six: Structure, Tectonics, and Geophysics*, Vol. 40, pp. 151–160, ed. Garry D. Mckenzie, AGU.

Muto, A., Peters, L.E., Gohl, K., Sasgen, I., Alley, R.B., Anandakrishnan, S. & Riverman, K.L., 2016. Subglacial bathymetry and sediment distribution beneath Pine Island Glacier ice shelf modeled using aerogravity and in situ geophysical data: new results, *Earth planet. Sci. Lett.,* **433,** 63–75.

Muto, A., *et al.*, 2019. Relating bed character and subglacial morphology using seismic data from Thwaites Glacier, West Antarctica, *Earth planet. Sci. Lett.,* **507,** 199–206.

O'Donnell, J., *et al.*, 2019a. Mapping crustal shear wave velocity structure and radial anisotropy beneath West Antarctica using seismic ambient noise, *Geochem. Geophys. Geosyst.*

O'Donnell, J., *et al.*, 2019b. The uppermost mantle seismic velocity structure of West Antarctica from Rayleigh wave tomography: insights into tectonic structure and geothermal heat flow, *Earth planet. Sci. Lett.,* **522,** 219–233.

O'Donnell, J.P. & Nyblade, A.A., 2014. Antarctica's hypsometry and crustal thickness: implications for the origin of anomalous topography in East Antarctica, *Earth planet. Sci. Lett.,* **388,** 143–155.

Piana Agostinetti, N. & Malinverno, A., 2018. Assessing uncertainties in high-resolution, multifrequency receiver-function inversion: a comparison with borehole data, *Geophysics,* **83**(3), KS11–KS22.

Pourpoint, M., Wiens, D., Shen, W., Aster, R.C., Nyblade, A. & Wilson, T.J., 2019. Constraints on shallow subglacial structure beneath Thwaites Glacier from joint inversion of receiver function and surface wave data, *AGUFM,* **2019,** NS11B–0632.

Ramirez, C., *et al.*, 2016. Crustal and upper-mantle structure beneath ice-covered regions in Antarctica from S-wave receiver functions and implications for heat flow, *Geophys. J. Int.,* **204**(3), 1636–1648.

Ramirez, C., *et al.*, 2017. Crustal structure of the Transantarctic mountains, Ellsworth Mountains and Marie Byrd Land, Antarctica: constraints on shear wave velocities, Poisson's ratios and Moho depths, *Geophys. J. Int.,* **211**(3), 1328–1340.

Randall, D.E. & Mac Niocaill, C., 2004. Cambrian palaeomagnetic data confirm a Natal Embayment location for the Ellsworth—Whitmore Mountains, Antarctica, in Gondwana reconstructions, *Geophys. J. Int.,* **157**(1), 105–116.

Reading, A.M., 2007. The seismicity of the antarctic plate, *Spec. Pap.-Geol. Soc. Am.,* **425,** 285.

Rignot, E., Mouginot, J. & Scheuchl, B., 2011. Ice flow of the antarctic ice sheet, *Science,* **333**(6048), 1427–1430.

Rudnick, R.L. & Fountain, D.M., 1995. Nature and composition of the continental crust: a lower crustal perspective, *Rev. Geophys.,* **33**(3), 267–309.

Schopf, J.M., 1969. Ellsworth mountains: position in West Antarctica due to sea-floor spreading, *Science,* **164**(3875), 63–66.

Shen, W., *et al.*, 2018. The crust and upper mantle structure of Central And West Antarctica from Bayesian inversion of Rayleigh wave and receiver functions, *J. geophys. Res.,* **123**(9), 7824–7849.

Siddoway, C.S., Baldwin, S.L., Fitzgerald, P.G., Fanning, C.M. & Luyendyk, B.P., 2004. Ross Sea mylonites and the timing of intracontinental extension within the West Antarctic rift system, *Geology,* **32,** 57–60.

Smith, A.M. & Murray, T., 2009. Bedform topography and basal conditions beneath a fast-flowing west antarctic ice stream, *Quater. Sci. Rev.,* **28**(7–8), 584–596.

Storey, B. & Dalziel, I., 1987. Outline of the structural and tectonic history of the Ellsworth Mountains-Thiel Mountains Ridge, West Antarctica, in *Gondwana Six: Structure, Tectonics, and Geophysics*, Vol. 40, pp. 117–128, ed. Garry D. Mckenzie, AGU.

Thybo, H. & Artemieva, I.M., 2013. Moho and magmatic underplating in continental lithosphere, *Tectonophysics,* **609,** 605–619.

Vaughan, D.G., Smith, A.M., Nath, P.C. & Le Meur, E., 2003. Acoustic impedance and basal shear stress beneath four antarctic ice streams, *Ann. Glaciol.,* **36,** 225–232.

von Frese, R.R.B., Tan, L., Woo Kim, J. & Bentley, C.R., 1999. Antarctic crustal modeling from the spectral correlation of free-air gravity anomalies with the terrain, *J. geophys. Res.,* **104**(B11), 25 275–25 296.

Wessel, P. & Smith, W.H., 1998. New, improved version of generic mapping tools released, *EOS, Trans. Am. Geophys. Un.,* **79**(47), 579–579.

Wilson, D.S. & Luyendyk, B.P., 2006. Bedrock platforms within the Ross Embayment, West Antarctica: hypotheses for ice sheet history, wave erosion, Cenozoic extension, and thermal subsidence, *Geochem. Geophys. Geosyst.,* **7**(12), doi:10.1029/2006GC001294.

Winberry, J.P. & Anandakrishnan, S., 2004. Crustal structure of the West Antarctic rift system and Marie Byrd Land hotspot, *Geology,* **32**(11), 977–980.

Zandt, G., Myers, S.C. & Wallace, T.C., 1995. Crust and mantle structure across the basin and range-Colorado Plateau boundary at 37 n latitude and implications for Cenozoic extensional mechanism, *J. geophys. Res.,* **100**(B6), 10 529–10 548.

SUPPORTING INFORMATION

Supplementary data are available at *GJI* online.

CKD_West_Antarctic_supplement.pdf

Figure S1. Forward modelling results at all ice stations. The best-fitting model is shown in a white star, and the 95 per cent confidence interval in white dashed.

Figure S2. Joint inversion results from all stations used in this study. Top left-hand panel: receiver functions at two maximum frequencies (0.5 and 2 Hz) stacked into narrow ray parameter bins (black) and the corresponding modelled receiver functions produced by the joint inversion (red). Bottom left-hand panel: Rayleigh wave phase velocity dispersion curve is shown in black and the best-fitting model in red. Right-hand panel: shear wave velocity–depth profile. The initial model is shown in black, best-fitting final model in red and 500 bootstrap iterations in grey. Dashed and dotted lines are shown at 4.0 and 4.3 km s^{-1}, respectively, to indicate mafic lower crust and the transition to upper mantle material. The interpreted Moho is shown with a black arrow.

Figure S3. Comparison between inversion results using just Rayleigh Wave phase velocity dispersion data (blue) and joint inversion using Rayleigh Wave phase velocity dispersion data and receiver functions (red) at station PIG3 using the same initial model. The interpreted Moho from both final models is shown by a blue arrow for the inversion only using dispersion data, and a red arrow for the joint inversion of receiver functions and dispersion data. Inversion just using dispersion data is not able to image the near surface structure associated with the ice layer, and also shows a gradational transition from crustal to upper mantle velocities. The joint inversion, which includes receiver functions and dispersion data, is able to resolve a clearer boundary between crustal and upper mantle velocities, which we interpret as the Moho. The inclusion of receiver functions in the inversion process clearly improves our resolution of sharp velocity discontinuities.

Figure S4. Comparison between using various V_p/V_s ratios in the joint inversion. In red is the joint inversion results presented in the manuscript, using the equations defined in Brocher (2005) to define V_p and density. In green is a joint inversion using a crustal V_p/V_s ratio of 1.80 and in blue a V_p/V_s ratio of 1.70. Although there is a slight difference in the shear wave velocity at each layer between the three models, all three curves agree within the bootstrap error bounds (grey), and the interpreted Moho would remain the same for all three (indicated by a black arrow). All receiver function waveform/dispersion curve model fits are very similar regardless of the V_p/V_s ratio used.

Figure S5. Panel (c) Running the bootstrap procedure with 1000 iterations (blue) and 500 iterations (grey). The bootstrap bounds are highly similar when run with 500 iterations versus 1000 iterations, as such we continue using 500 iterations given the reduced computation time.

Table S1. Table of results from all stations used in this study. Ice thickness is from BEDMAP2 (Fretwell *et al.* 2013). ∗Subglacial sediment results used from Chaput *et al.* (2014) at UPTW due to unstable solution in forward modelling. The tectonic block/region acronyms are as follows: Antarctic Peninsula (AP), Ellsworth Land (EWL), Haag-Ellsworth Whitmore (HEW) and West Antarctic Rift System (WARS).

Please note: Oxford University Press is not responsible for the content or functionality of any supporting materials supplied by the authors. Any queries (other than missing material) should be directed to the corresponding author for the paper.